Dissecting the Contributions to Non-photochemical Quenching in a Land Plant Under Fluctuating Light

Graham Fleming
grfleming@lbl.gov
University of California, Berkeley https://orcid.org/0000-0003-0847-1838
Lam Lam
University of California, Berkeley
Rebecca Lee
University of California, Los Angeles https://orcid.org/0000-0002-6274-1328
Dhruv Patel-Tupper
UC Berkeley https://orcid.org/0000-0002-0642-1485
Henry Lam
University of California, Berkeley
Tsung-Yen Lee
University of California, Berkeley
Alexa Ma
University of California, Berkeley
Sophia Ma
University of California, Berkeley
Hetty He
University of California, Berkeley
Krishna Niyogi
University of California, Berkeley https://orcid.org/0000-0001-7229-2071

Article

Keywords:

Posted Date: May 20th, 2025

DOI: https://doi.org/10.21203/rs.3.rs-6430823/v1

Additional Declarations: There is **NO** Competing Interest.

Version of Record: A version of this preprint was published at Nature Communications on March 9th, 2026. See the published version at https://doi.org/10.1038/s41467-026-70414-2.

Dissecting the Contributions to Non-photochemical Quenching in a Land Plant Under Fluctuating Light

Lam Lam[1,2]†, Rebecca Lee[3]†, Dhruv Patel-Tupper[2,4], Henry E. Lam[5], Tsung-Yen Lee[2,5], Alexa Ma[5], Sophia A. Ma[4], Hetty He[9], Krishna K. Niyogi[2,4,6,7]and Graham R. Fleming[1,2,5,8*]

[1]Graduate Group in Biophysics, University of California, Berkeley, CA 94720, USA.

[2]Molecular Biophysics and Integrated Bioimaging Division, Lawrence Berkeley National Laboratory, Berkeley, CA 94720, USA.

[3]Department of Chemistry, University of California, Los Angeles, CA 90095, USA.

[4]Department of Plant and Microbial Biology, University of California, Berkeley, CA 94720, USA.

[5]Department of Chemistry, University of California, Berkeley, CA 94720, USA.

[6]Howard Hughes Medical Institute, University of California, Berkeley, CA 94720, USA.

[7]Innovative Genomics Institute, University of California, Berkeley, CA 94720, USA.

[8]Kavli Energy Nanoscience Institute, Berkeley CA 94720, USA.

[9]Department of Molecular and Cell Biology, University of California, Berkeley, CA 94720, USA.

†These authors contributed equally.

*Corresponding authors. E-mail: grfleming@lbl.gov

ABSTRACT

To safely dissipate excess excitation energy, photosynthetic organisms have evolved multiple photoprotection mechanisms. These mechanisms involve various molecular players functioning on overlapping timescales from seconds to days, making it challenging to isolate and quantify their individual kinetics. In this study, we perform whole-leaf chlorophyll fluorescence lifetime and xanthophyll concentration measurements on wild-type and various newly characterized non-photochemical quenching mutants of *Nicotiana benthamiana*, an allotetraploid vascular land plant. Based on these measurements, we construct a fluorescence lifetime-based quantitative kinetic model that disentangles individual photoprotection components and, when integrated additively, accurately predicts wild-type and mutant quenching/recovery behaviors under various light-dark regimes. Additionally, the model quantifies the per-molecule quenching efficiencies of various xanthophylls and the contributions of six quenching pathways across different mutants. It also suggests that enhancing VDE, ZEP, and PsbS expression improves overall quenching efficiency, aligning with previous studies and supporting translational efforts to optimize photoprotection and enhance crop yields under dynamic light environments.

INTRODUCTION

The initial step in photosynthesis involves the absorption of a photon and excitation of chlorophyll to its singlet excited state (^{1}Chl*) within light-harvesting complexes (LHCs), facilitating electronic energy transfer to the reaction center (RC) to drive charge separation[1]. However, under high light conditions, the photosynthetic electron transport chain can become saturated. When ^{1}Chl* lacks an adequate electron acceptor, formation of the longer-lived triplet state of chlorophyll (^{3}Chl*) via intersystem crossing can occur[2]. These triplet states, when interacting with molecular oxygen, produce reactive oxygen species (ROS), which pose a threat to thylakoid membrane integrity by damaging essential pigments, proteins, and lipids[3,4]. To prevent or mitigate such damage, oxygenic photosynthetic organisms have evolved multiple sophisticated photoprotection pathways, collectively known as non-photochemical quenching (NPQ) mechanisms, to safely dissipate excess excitation energy as heat[5,6].

To date, five distinct NPQ mechanisms have been discovered, with various genetic mutants deepening our understanding of land plant NPQ at the molecular level. Among these mechanisms, energy-dependent quenching (qE) occurs on a seconds-to-minutes timescale and accounts for the majority of NPQ induction and relaxation in response to dynamic light intensity changes[7]. qE involves the coordinated action of a pH-sensing protein photosystem II subunit S (PsbS/NPQ4)[8,9] and xanthophyll carotenoids, primarily zeaxanthin (Zea, Z) and lutein (Lut, L). Under high light conditions, violaxanthin de-epoxidase (VDE/NPQ1) coverts violaxanthin (Vio, V) to antheraxanthin (Ant, A) and subsequently to Zea, a process reversed by zeaxanthin epoxidase (ZEP/NPQ2) under low light/dark conditions[10,11]. Lut, produced via lycopene epsilon cyclase (LUT2), independently and additively contributes to NPQ along with Zea[12,13], however the relative contributions of each carotenoid to qE are still extensively debated [11,12,14,15].

The longer-lasting Zea-dependent quenching mechanism (qZ) functions independently of PsbS, which is required for qE[16]. Unlike canonical NPQ mechanisms, state transitions in light-harvesting complex II (qT) regulate light harvesting by redistributing excitation energy between photosystem I (PSI)

and photosystem II (PSII)[17]. Since qT does not directly quench ^{1}Chl*, it contributes minimally to the overall fluorescence quenching in the organism studied here, *Nicotiana benthamiana*. The most slowly relaxing NPQ component, photoinhibition (qI), occurs when photoprotection is insufficient, resulting in the hours to days long photoinactivation of PSII[18]. Collectively, these NPQ mechanisms involve diverse molecular players that function either additively or independently across overlapping timescales to acclimate to varying illumination conditions in nature. This makes it challenging to disentangle and study their individual kinetics and contributions *in vivo*[19].

In previous studies[20,21], a xanthophyll cycle-based kinetic model of short-term photoprotection was developed in the alga *Nannochloropsis oceanica*. This model, utilizing Chl fluorescence lifetime and xanthophyll concentration measurements, captured the dynamics of xanthophyll interconversion and quenching activity, and further highlighted Zea as the most effective photoprotective carotenoid quencher, followed by Ant and Vio. The model also predicted the behavior of two mutants that were not included in the parameterization of the model[21]. These findings provided valuable insights into the kinetics of fast-reacting photoprotection and implications for optimizing photosynthetic efficiency.

However, this model had a number of significant limitations: First, the model was based on a definition of NPQ capacity analogous to the generally used definition based on fluorescence intensity ($NPQ = \frac{Fm - Fm'}{Fm'}$, or $NPQ_\tau(t) = \frac{\tau_{dark}(t=0) - \tau(t)}{\tau(t)}$) and, in the latter, calculated using Chl fluorescence lifetimes measured in "snapshots" over time as quenching in excess light or relaxation in darkness occurs. Here $\tau_{dark}\ (t = 0)$ denotes the amplitude-weighted average lifetime of the initial dark snapshot, and $\tau(t)$ denotes the lifetime at the corresponding snapshot sequence time t. While convenient for modeling, normalization by the initial dark-acclimated lifetime $\tau_{dark}\ (t = 0)$ forces the assumption of zero initial quenching in the darkness, which may not hold in mutants with impaired NPQ recovery or altered thylakoid protein composition, such as *zep* or *lut2* mutants. This limits the comparability of the NPQ_τ parameter across different genotypes with differing initial fluorescence lifetimes. Additionally, its dependence on $\tau(t)$ becomes nonlinear at high quenching levels, hence its relationship to true quenching

dynamics becomes unclear. In particular, the model assumes that NPQ_τ is directly proportional to the concentrations of quenching species, which is not true for NPQ_τ levels > 2. To address this issue, we formulated the model in this study to directly fit the measured Chl fluorescence lifetimes, allowing for a more fundamental and accurate representation of NPQ capacity.

Second, *Nannochloropsis oceanica* lacks specific pigments found in land plants, such as Lut and chlorophyll *b* (Chl *b*), and relies on the phylogenetically and functionally distinct algal protein LHCXI, rather than PsbS, to initiate qE[22–24]. Consequently, the model is not directly applicable to land plants. This limitation is particularly significant given the long-standing debate regarding the roles of Zea and Lut as quenchers in qE, as well as their potentially distinct quenching kinetics and mechanisms[25]. In addition, while the previous model incorporated qZ, it did not include qI—the slowest NPQ component—which is present at substantially higher relative magnitudes in plants but is challenging to disentangle from other mechanisms[19,26]. Therefore, developing a new lifetime-based model tailored to land plants that includes both the Lut-dependent qE quenching pathway and qI is essential to provide deeper insights into these debates and improve our capability to predict and engineer NPQ in plants.

In this study, we systematically investigate the NPQ response using a comprehensive set of single and double NPQ mutants[25] in *N. benthamiana* (**Table 1**) across three regular/irregular actinic light sequences. By combining five critical mutants, each lacking specific components of the NPQ pathways, we construct a lifetime-based quantitative kinetic model of NPQ (encompassing qE, qZ, and qI). Model parameters are directly fitted to the experimental Chl fluorescence lifetimes, guided by xanthophyll concentrations measured via high-performance liquid chromatography (HPLC). Parameterized using four single mutants and one double mutant under fluctuating light, this approach enables us to isolate the activation and relaxation kinetics of NPQ as well as the contributions of each mechanism individually while capturing their interplay—the model accurately predicts NPQ responses in the four single mutants under constant light, as well as the wild type (WT) and four additional double mutants under three different illumination sequences. Furthermore, the model enables comparisons of per-molecule quenching

efficiencies of the xanthophylls and gives further prediction of quenching kinetics with overexpression of VDE, PsbS, and/or ZEP in various stoichiometries. Altogether, these findings highlight potential strategies to modulate key enzyme expression and activity, offering valuable insights for enhancing NPQ efficiency and improving crop productivity[27,28].

RESULTS

An NPQ kinetic model based on chlorophyll fluorescence lifetime

We aimed to construct a minimal model of NPQ dynamics in land plants derived from known biochemical processes. Our kinetic model incorporates three key components: a dynamic xanthophyll cycle, lutein activation, and a simplified phenomenological representation of qI. The model incorporates 13 chemical species: free xanthophylls Vio (V)/Ant (A)/Zea (Z), protein-xanthophyll bound complexes PV/PA/PZ, and an additional protein-Lut complex PL, which are activated to be quenching complexes (QX) in light, as well as the key xanthophyll cycle enzymes VDE and ZEP. A phenomenological representation of qI is given by modeling α_{qI}, the ratio of damaged reaction centers to the whole pool. A simplified schematic of this model is shown in **Figure 1A** and a detailed description is provided in the Methods section.

To address the limitations of our previous *N. oceanica* model described in the Introduction and expand the model to represent land plant NPQ, we present an alternative approach to directly model quenching using the fundamental definition of fluorescence lifetime. The total fluorescence decay rate, $\tau_F(t)$, is determined by several competing processes, including the non-radiative decay and the intrinsic fluorescence decay of Chl *a*, qE, qZ, and qI. Assuming the quenching rate is linearly dependent on the concentration of quenching species, we define the fluorescence lifetime of Chl *a* via a Stern-Vollmer type approach as:

$$\frac{1}{\tau_F} = \kappa_{r,nr} + \kappa_{qE}[QX] + \kappa_{qZ}[Z] + \kappa_{qI}[I] \quad (1)$$

Where $\kappa_{qE,}$ $\kappa_{qZ,}$ κ_{qI} represent the quenching rate constants of qE, qZ, and qI, respectively, and $\kappa_{r,nr}$ accounts for all the other radiative and non-radiative de-excitation processes. Furthermore, since QV, QA, QZ, and QL may exhibit different per-molecule quenching efficiencies, we further distinguish their contributions within qE:

$$k_{qE}[QX] \approx \kappa_{QV}[QV] + \kappa_{QA}[QA] + \kappa_{QZ}[QZ] + \kappa_{QL}[QL] = \sum_X \kappa_{QX}[QX] \quad (2)$$

This yields the final time-dependent expression for the Chl *a* fluorescence lifetime:

$$\tau_F(t) = \frac{1}{k_{r,nr} + \sum_X \kappa_{QX}[QX] + \kappa_{qZ}[Z] + \kappa_{qI}\alpha_{qI}} \quad (3)$$

This formulation allows for direct quantification of quenching rates and per-molecule efficiencies of the individual quenchers while accounting for genotypic variations in τ_{dark} $(t = 0)$. In this model, $\kappa_{qX,}$ $\kappa_{qZ,}$ and κ_{qI} are additional fitting parameters, while $k_{r,nr}$ is calculated directly from τ_{dark} $(t = 0)$ for each mutant. Details of the model implementation and fitting are given in Methods and Supplementary Information (Extended Methods).

Characterization of xanthophyll cycling in novel NPQ mutants of *N. benthamiana*

To systematically disentangle the individual quenching pathways found in *N. benthamiana*, we characterized a series of mutants, each deficient in one or more NPQ mechanisms. Three such mutants were characterized previously: the *psbs1 psbs2* mutant which lacks qE (hereafter *npq4*), the *lut2-1 lut2-2* mutant which lacks lutein-dependent qE (hereafter *lut2*). And the *vde1 vde2* mutant which lacks qZ (hereafter *npq1*)[25]. In this study, we generated and characterized single and double mutants deficient in one or both ZEP orthologs. Given the near lethality of the *zep1zep2* double knockout in *N. benthamiana,* only one of eleven T_0 transformants produced viable, stable progeny (see Methods). Each ortholog contributes additively to Zea epoxidation, with ZEP1 being the dominant copy. Interestingly, knockout of ZEP2 (hereafter *zep2*) retains a near-native Vio and Neo composition, with sufficient constitutive Zea to saturate

Zea-dependent qE capacity (**Fig. S1**), unlike the non-native composition found in the *A. thaliana npq2* mutant[10]. This *zep2* mutant provided quantitative and temporal variation in Zea-dependent qE and qZ necessary and sufficient for phenotypic modeling.

The presence or absence of these traits within the canonically described qE, qZ, and qI parameters that represent a vast majority of WT land plant NPQ are included in **Table 1**. These mutants enabled a stepwise model training approach, where parameters were progressively fitted, starting with the simplest NPQ system (*npq4npq1*, which contains only qI) and gradually incorporating additional quenching components to reconstruct the full WT model (**Fig. 1B**). Whole-leaf pigment profiles were quantified using HPLC under dark-acclimated and high light (HL)-acclimated conditions for all genotypes used in this study (**Fig. S2**). WT, *npq4, zep2, lut2,* and *zep2lut2* mutants exhibited robust de-epoxidation of Vio in response to HL, and furthermore, *zep2, npq4zep2* and *zep2lut2* retained more residual accumulation of Ant and Zea in the dark and after HL due to reduced ZEP activity. On the contrary, *npq1* and its double mutants (*npq1npq4, npq1lut2*) displayed no significant changes in pigment profiles before and after HL exposure, indicating a complete loss of VDE function[29–31]. Additionally, *lut2* and its derived double mutants (*npq4lut2, npq1lut2, zep2lut2*) lacked detectable Lut and exhibited a considerably expanded VAZ pool size, consistent with previous reports[32].

Training the NPQ model with chlorophyll fluorescence lifetimes

Whole-leaf Chl fluorescence lifetime measurements were conducted using time-correlated single-photon counting (TCSPC), as described in detail in the Methods section. The genotypes *npq4npq1*, *npq4*, *npq1*, *lut2*, and *zep2* are the minimal set sufficient to fit all parameters, integrating all major photoprotective pathways in order to reconstruct the complete WT model of τ_F (**Fig. 1B**). Fluorescence lifetime data was collected using a 5HL-10D-5HL actinic light sequence (**Fig. 2A–E**). In general, fluorescence lifetimes decreased during the light period, indicating quenching activity, and increased to varying extents in *npq4*, *npq1*, *lut2*, and *zep2* during the following dark period, reflecting partial NPQ recovery. Among these, *lut2* and *zep2*, both possessing functional VDE and therefore Zea as a quencher, exhibited shorter lifetimes

compared to *npq1*, which lacks Zea. Conversely, *npq4npq1* and *npq4*, both deficient in PsbS, showed less quenching and minimal recovery.

Our model fitting results (**Fig. 2A–E**) successfully captured the contributions of individual quenching species—*npq4npq1* for qI, *npq4* for qZ, and *npq1* for Vio-dependent qE (qE_V) and Lut-dependent qE (qE_L)—as well as the combined effects of multiple quenchers (*lut2*, *zep2*). Except for the initial Vio concentration, which was derived from HPLC results, all fitting parameters remained consistent across mutants. While the qI component was derived from fitting *npq4npq1* lifetime data under the 5HL-10D-5HL sequence (**Fig. 2A**), an additional control measurement performed using only laser excitation without actinic light on *npq4npq1* (laser baseline) was accurately captured by the qI-only model (**Fig. S3**). This indicates although the laser baseline modestly contributes to detectable quenching, this effect is accounted for in our model within the qI parameters via the positive α_{qI} accumulation rate in darkness in *npq4npq1*.

In *npq4* (**Fig. 2B**), the relatively slow activation and relaxation dynamics were attributed to the slower qI and qZ mechanisms. In *npq1* (**Fig. 2C**), the NPQ components qI, qE_V, and qE_L exhibited rapid activation, contributing to an initial sharp decrease in lifetime, although the model slightly underestimated lutein activation rates. Partial recovery in the dark period was attributed to the rapid deactivation of qE_L. Similarly, *lut2* (**Fig. 2D**) exhibited substantial contributions to activation from qE_V, as well as Ant-dependent qE (qE_A), and Zea-dependent qE (qE_Z), with lingering qZ causing a prolonged relaxation phase in the dark. In *zep2* (**Fig. 2E**), the rapid initial NPQ activation was largely driven by pre-existing Zea, leading to a strong qE_Z followed by a slower qZ response. Partial recovery in darkness resulted from qE_Z deactivation, while qZ recovery remained slow. Similar model fitting accuracy was observed under the 3HL-1D-1HL-3D-9HL-3D sequence (**Fig. S4**).

To ensure consistency of rate parameters across genotypes, fluorescence lifetime datasets were fitted in batches. In the absence of Lut, which plays a critical role in maintaining trimeric LHCII stability, *lut2* mutants have altered LHCII pigment compositions (e.g. replacement of Lut by Vio, Ant, and Zea)

and xanthophyll binding affinities, which will affect excitation energy quenching[25,31]. As a result, kinetic rate parameters for PX formation specific to *lut2* were used and marked by an asterisk (*). Additionally, to account for genotypic differences in pigment composition, initial pigment concentrations V_0 were fitted independently for each genotype.

The kinetic parameters obtained from *npq1*, *npq4*, *lut2*, *zep2*, *npq1npq4*, and WT under HL conditions are summarized in **Table S1**. In *zep2*, the conversion of Z to A and A to V was reduced because of lower ZEP activity due to knockout of the less dominant of two ZEP paralogs, thus ZEP function was not entirely eliminated. Large rate constants for the formation of protein-xanthophyll complexes PX, denoted by $X + P \rightleftharpoons PX$, reflect a rapidly equilibrating process, whereas the formation from PX to quenching complexes QX occurred at a much slower rate, influencing NPQ induction dynamics. QL shows a similar per-molecule activation rate to QV but substantially lower than QZ and QA. However, given its high concentration relative to the VAZ pigments, the contribution of QL to overall quenching is nevertheless significant. The total number of VAZ binding sites, $[P]_{tot}$, is approximately halved in *lut2*, consistent with the importance of Lut as a structural component of the LHCII trimer.

Quenching rate constants for each xanthophyll species are provided in **Table S2**. The quenching rate (k_X) for a given species X is defined as $k_X = \kappa_{QX}[X]$, where κ_{QX} represents quenching rate constant and $[X]$ represents the concentration of the quenching species (in mmol/mol Chl). These rate constants (κ_{QX}) reflect intrinsic differences in quenching ability between the pigments once activated. Though κ_{qZ} is substantially lower than κ_{QZ}, $[Z]$ typically exceeded $[QZ]$ by an order of magnitude, so the overall quenching contributions of qZ and qE_Z are similar. The quenching rate constants for Lut and Zea are also similar, with Lut being slightly higher. κ_{qI} acts on the fractional quantity α_{qI}; thus, the rate of photoinhibition does not exceed 2.82 (mmol/mol Chl^{-1} s^{-1}) in this model.

Predictions made by the NPQ model

To assess the predictive capabilities of our kinetic model, we performed fluorescence lifetime measurements on WT and an additional set of *N. benthamiana* mutant leaves under three distinct illumination sequences, as described above. Parameters obtained by fitting the previous five mutants were integrated without modification to construct a complete WT model (only $[V]_{0,WT}$ was fitted separately). Across all illumination sequences, the model successfully captures the overall kinetics of NPQ induction and relaxation in WT leaves (**Fig. 3A-C**). In particular, the model captures the WT characteristics of slower initial activation of NPQ, partial recovery in dark, and fast activation upon re-illumination. Consistent with our current understanding of *N. benthamiana* photoprotection, the model predicts a strong reliance on qE and qZ under continuous and fluctuating high light conditions, reflecting the dominant role of these mechanisms in rapid adjustment to fluctuating light and acclimation to intense light stress.

While the model accurately reproduces NPQ dynamics in the 5HL-10D-5HL and 20HL sequences, it slightly underestimates NPQ activation during the first ~8 min of the irregular 3HL-1D-1HL-3D-9HL-3D sequence. This discrepancy likely arises from biological variability, such as differences in VAZ pool sizes, growth conditions, or leaf-to-leaf variation. Such factors, which may contribute to batch-dependent discrepancies, are further discussed in the Discussion.

Beyond WT, the model effectively captures NPQ dynamics in the four single mutants *npq1*, *npq4*, *lut2*, *zep2* measured under 20-min HL (**Fig. S5**), as well as an additional set of double mutants, including *zep2lut2, npq1lut2, npq4lut2, npq4zep2* in the 5HL-10D-5HL sequence (**Fig. 3D-G**), with only a slight overestimation of quenching in *npq4zep2* during the later phases of the illumination sequence. This overestimation may result from differences in ZEP levels and total VAZ pool sizes between *zep2* and *npq4zep2* mutants (**Fig. S2**) or could simply result from biological variation, as described further in the Discussion. The model also gives reasonable predictions of NPQ behavior in these four double mutants under the 3HL-1D-1HL-3D-9HL-3D sequence (**Fig. S6**). These findings highlight the model's robustness in integrating multiple quenching components.

The agreement between experimental data and model predictions for WT, four single mutants (under 20HL), and four double mutants under different illumination sequences support the validity of the kinetic parameters obtained from fitting and the model's underlying assumptions. In particular, the model accurately predicts WT induction and relaxation dynamics from a direct sum of the individual quenching pathways associated with qE_V, qE_A, qE_Z, qE_L, qZ, and qI, demonstrating that the effects of these mechanisms can be distinguished from each other and may be considered additive. The generalizability of the kinetic parameters to single mutants (20HL) and double mutants further supports our hypothesis that the NPQ mechanisms are distinguishable, and that each quenching mechanism operates largely independently so that even double knockouts retain the NPQ capabilities from the remaining pathways, although all four qE mechanisms require PsbS. Additionally, the model makes accurate predictions of *lut2* double mutants using the *lut2*-specific PX binding rates, consistent with the effect of Lut on the stability of LHCII trimeric structure[25,31].

DISCUSSION

NPQ mechanisms play a critical role in regulating photosynthetic efficiency and protecting plants from photodamage[7,33]. Here, we present a novel theoretical framework that models NPQ dynamics by directly predicting Chl fluorescence lifetime, with fitting parameters constrained by xanthophyll concentrations. With a series of newly characterized NPQ mutants in *N. benthamiana*, we are able to independently extract Vio/Ant/Zea-dependent qE, Lut-dependent qE, qZ and qI. Using a parameterized approach to capture photoprotective dynamics, the model offers predictive insight into both fluorescence lifetime kinetics and xanthophyll concentration in *N. benthamiana*.

The success in reconstructing the WT NPQ response from the individual mutant data implies that the various contributions to overall NPQ are linear and additive. It is also important to note that basing the analysis on fluorescence lifetimes via a Stern-Volmer approach was critical to obtaining transferable

parameters. The non-linear relationship of the conventional NPQ definition ($NPQ = \frac{Fm - Fm'}{Fm'}$, or $NPQ_\tau(t) = \frac{\tau_{dark}(t=0) - \tau(t)}{\tau(t)}$) and the variability of the initial dark (reaction centers closed) fluorescence lifetime would significantly compromise an approach based on conventional NPQ values. Another key assumption of our modeling approach is that the elementary reaction rates underlying each NPQ mechanism remain consistent across different genotypes and that the phenotypic effect of a single mutant remains the same in its corresponding double mutant. While pleiotropic effects of mutations could influence some of these parameters, this assumption is validated by the accurate prediction of most double mutant lifetimes (**Fig. 3 D-G**), and the predictive power of the rates obtained through fitting mutant data suggests a reasonable level of confidence in their values, demonstrating the model's overall robustness.

The kinetic parameters obtained from our model provide a quantitative basis for comparing the relative efficiencies of key NPQ processes across different xanthophylls. Our results indicate that the formation of PX complexes occurs significantly faster than their subsequent activation into quenching states QX, in agreement with previous findings[20,21]. However, comparatively, zeaxanthin exhibits the fastest rate of forward PZ formation, as well as the highest equilibrium ratio of bound PZ to free Z (given by $\frac{k_{pxf}}{k_{pxf}+k_{pxb}}$), whereas violaxanthin has the slowest formation and lowest ratio of PV to V (**Table S1**). Although PV/PA/PZ formation is generally slower in *lut2* as discussed previously, the forward PX conversion rates and equilibrium ratios for Vio/Ant/Zea still favor zeaxanthin. Similarly, the forward rate of QX activation is highest for zeaxanthin. Together, these results suggest that the preference for Zea as a quencher originates not only from its inherent molecular quenching ability, but also its favorability in binding to light-harvesting complexes and forming the active quenching complex, possibly with PsbS. Interestingly, the backward conversion from QX to PX is faster for Zea and Ant compared to Vio, suggesting that QV is both slow to form and slow to deactivate. However, given the extremely low concentrations of QV, the precision of these fitted rates is expected to be lower than that of QA and QZ.

In addition, the activation rate of QL is similar to that of QV; however, the considerably higher concentration of lutein allows QL to still form in substantial amounts.

Our model also provides insights into the kinetics of xanthophyll cycle interconversion. Under HL conditions, the estimated rate of Vio-to-Ant conversion is faster than Ant-to-Zea conversion, which appears to contrast with conclusions from the previous *Nannochloropsis* model[21], where A-to-Z conversion was reported as the faster de-epoxidation step. Since no mutant isolates Ant from Zea quenching, fully distinguishing its quenching kinetics from Zea remains challenging. Future studies using engineered enzyme variants could help refine these estimates.

In addition, the model allows for a direct comparison of the quenching efficiency per molecule for each xanthophyll species to the total amount present, which we define as:

$$Q_{eff} = \frac{k_{pxf}}{k_{pxf}+k_{pxb}} \cdot \frac{k_{qxf}}{k_{qxf}+k_{qxb}} \cdot \kappa_{QX} \quad (4)$$

where quenching efficiency is determined by (1) the fraction of pigment X bound to a protein site, (2) the maximum fraction of bound protein-xanthophyll complex PX that activate as quenchers QX under light conditions, and (3) the quenching rate constant of QX. The estimated quenching efficiencies obtained from the WT model are given in **Table 2**. The model reports Zea in the form of qZ and QZ to be the strongest quenchers and Vio (QV) to be the weakest quencher, while Ant (QA) shows intermediate quenching efficiency, in line with our current understanding of the relative strength of Vio/Ant/Zea as quenchers. QV, QA, and QZ have an approximately 1:3:30 ratio of quenching efficiencies, a relative increase in the quenching ability of zeaxanthin compared to a previous study[21]. This may reflect inherent differences in NPQ mechanism details between land plants and algae. The per-molecule quenching efficiency of Lut is similar to Ant. Thus, Zea (both qZ and QZ) generally exhibits a quenching efficiency 10 times that of Lut, in agreement with previous studies[34]. However, since Lut is generally present in considerably higher concentrations than zeaxanthin, the absolute quenching contributions of Zea and Lut are similar on short timescales.

The quenching rate constants and per-molecule quenching efficiency Q_{eff} obtained from our model provide a quantitative basis for comparing the relative efficiencies of key NPQ processes across different xanthophylls. Formulating our modeled quenching rates in terms of quenching rate constants times concentrations ($\kappa_{QX}[X]$) allows us to quantify the differing quenching abilities of the key components of the photoprotective system in a time-dependent manner following exposure of the leaf to excess light (**Figure 4, Movie S1**). Based on model predictions, over the course of 20 min of HL exposure, photoinhibition increases in all genotypes, although those with strong NPQ capabilities show slower qI accumulation, as expected. In WT, at t < 1 min (**Figure 4A**), Lut and Vio are the major quenching contributors due to their rapid activation capabilities. Within 3 min (**Figure 4B**), Ant contributes substantially to quenching, and after 5 min (**Figure 4C**), Zea is the main quenching contributor. After 20 min (**Figure 4D**), Zea is overwhelmingly dominant, suggesting that Zea is the most important player in long-term defense against light stress. A similar pattern is observed in *lut2* and *zep2*, albeit accelerated in *zep2* due to the pre-existing presence of Zea in the dark, and without Lut contributions in *lut2*. In *npq1*, lack of the VDE-mediated VAZ cycle results in increased Vio quenching. In *npq4* and *npq1npq4*, which lack most major NPQ pathways, qI accumulates at an increased rate.

The complete WT model further provides a framework for guiding systematic modifications to *N. benthamiana* to improve NPQ induction and relaxation dynamics, ultimately aiming to increase crop yields. In particular, overexpression of VDE, ZEP, and PsbS has been shown to increase biomass in certain species (*N. tabacum* and soybean/*G.max*), hypothetically by maintaining a WT level of quenching under high light while enabling faster relaxation in low light or darkness[35,36]. However, similar enhancements were not observed in *A. thaliana* and potato/*S. tuberosum*[37,38]. While the reasons for these species-specific discrepancies remain unclear[39], some studies suggest that optimizing the stoichiometries of these three proteins is crucial, depending on their native qE and qZ capacities, to achieve both faster, but not greater, quenching under high light and, more importantly, enhanced recovery in darkness[36,39,40]. Using our model, we investigate different expression levels and overexpression ratios of these key

enzymes. VDE and ZEP overexpression is modeled by increasing $k_{va/az}$ and $k_{za/av}$ respectively. PsbS overexpression is modeled by increasing the PsbS-dependent rate k_{QX} by the same factor across all xanthophylls. Model predictions (**Fig. 5**) suggest that inducing a 2:10:1 expression ratio of VDE to ZEP to PsbS enhances both NPQ activation and relaxation rates and amplitudes. Additionally, overexpressing ZEP and PsbS by five- and two-fold. respectively, results in NPQ behavior considered optimal for improving crop yield—achieving faster but equal quenching in HL while allowing greater recovery in darkness compared to WT[35]. In these modeled VPZ overexpression mutants, an increase in the relative contribution from qE_V, qE_A, qE_Z, and qE_L is responsible for the improvement of induction/recovery. Future experimental work with VPZ mutants of *N. benthamiana* or closely related species will be necessary to validate these predictions.

While the kinetic model presented here successfully captures NPQ dynamics in *N. benthamiana*, several limitations must be considered. Biological variation introduces uncertainty in parameter estimation, as differences in growth conditions and leaf age affect pigment pools, enzyme activity, and consequently, fluorescence lifetime and xanthophyll interconversion rates—even within the same genotype. These factors likely contribute to the model's slight NPQ underestimation in the 3HL-1D-1HL-3D-9HL-3D sequence (**Fig. 3C**). While biological replicate averaging and normalization in this model (using $\tau_F(0)$ as an initialization parameter) help mitigate variability, fully resolving it remains challenging. In addition, the model also simplifies the illumination treatments, focusing on HL-to-D transitions rather than the HL-to-low-light (LL) fluctuations common in nature[41]. More gradual transitions could influence both the relative contributions and the relaxation kinetics of different NPQ components. Additionally, the interplay between light intensity and NPQ induction—particularly the threshold-dependent activation of different molecular players—remains an open question[42]. Incorporating HL-LL transitions and light intensity-dependent rate constants may improve the physiological relevance of this framework for understanding NPQ regulation under natural light fluctuations, if not offset by increased phenotypic variability.

Despite these limitations, the model provides a valuable quantitative framework for dissecting NPQ mechanisms in land plants. Its ability to resolve the contributions of different quenchers and predict both fluorescence lifetime and xanthophyll dynamics suggests it can serve as a foundation for future refinements, improving predictions on the impact of key genetic modifications on NPQ dynamics and crop yields.

METHODS

Plant Material and Growth Conditions

Transgenic *Nicotiana benthamiana* (accession *Nb-1*) lines were generated via *Agrobacterium*-mediated transformation by the Ralph M. Parsons Foundation Plant Transformation Facility at UC Davis (https://ptf.ucdavis.edu/), as described in a previous work[25]. The newly characterized *zep2* mutant was generated using the same approach, with the guide RNAs listed in **Table S3**. Higher-order quadruple mutants were generated by crossing homozygous double mutants (e.g. *npq4* or *psbs1 psbs2* crossed with *npq1* or *vde1 vde2*). Progeny were screened and genotyped to identify homozygous mutants with the appropriate mutations, as described below. *N. benthamiana* plants were grown with a 10-hour daylength in a south-facing greenhouse. Seeds were germinated directly on a mixture of four parts Sunshine Mix #1 (Sungro) and one part perlite. Plants were fertilized with JR Peter's Blue 20-20-20 fertilizer monthly.

Genotyping of CRISPR/Cas9 Edits

Genomic DNA from putative knockout lines was isolated and genotyped by Phire Plant Direct PCR Master Mix (ThermoScientific™, Catalog #F160L) using the supplied dilution buffer. DNA was amplified by PCR using primers that spanned the two gRNA target sites for each gene of interest, with primer pairs specific to one of the two highly similar paralogs**.** PCR products were purified and sequenced

by Sanger sequencing using the primers listed in **Table S4**. The knockout alleles for single trait and higher order mutants are listed in **Table S5** and **Table S6**, respectively. Segregation of the Cas9 transgene was determined via changes in chlorophyll fluorescence after antibiotic treatment as previously described[43].

High-performance Liquid Chromatography of Whole-Leaf Extracted Pigments

Leaves were harvested from *Nicotiana benthamiana* plants that had been dark-acclimated overnight and were cut into equal-sized disks (~0.5 cm). These leaf disks were exposed to dark or light conditions (~1500 µmol m^{-2} s^{-1}) under a white-light LED panel. Each leaf disk was flash-frozen in liquid nitrogen, collected in tubes containing Lysing Matrix D beads and homogenized using a High-Speed Homogenizer (6.0 m/s, 1 × 40 s; FastPrep-24 5G™; MP Biomedical). Pigments were extracted twice with 200 µL 100% ethanol until the remaining leaf debris, pelleted after 14,000rpm centrifugation for 5 mins, turned white to ensure complete extraction. To minimize pigment degradation and solvent evaporation, the extraction process was performed on ice or at 4°C and in the dark. Approximately 400 µL of the pigment solution was collected from each sample, filtered through a 0.2 µm nylon filter, and concentrated to ~150 µL under nitrogen flow for 5 minutes before loading into an HPLC vial. The total leaf-pigment profile, including neoxanthin, violaxanthin, antheraxanthin, lutein, chlorophyll-*b*, zeaxanthin, chlorophyll-*a*, and β-carotene, was obtained by performing high-performance liquid chromatography (1100 HPLC, Agilent) with a combination of solvents consisting methanol, methyl-*tert*-butyl ether and water[44] for **Figure S1** or a C30 column (YMC Carotenoid, 5 µm, YMC America) with a gradient of solvents consisting methanol, methyl-*tert*-butyl ether and water[45] for **Figure S2**. Pigments were quantified against standard dilution series.

Whole-leaf Fluorescence Lifetime Measurements and Analysis

We used a lab-constructed time-correlated single photon counting (TCSPC) setup, similar to a previously described design[19], to measure Chl fluorescence lifetimes and quantify the quenching kinetics of the leaf samples. A diode laser (Coherent Verdi G10) operating at ~532nm was used to pump a Ti:sapphire oscillator (Coherent, Mira900f, 76 MHz), generating pulses centered at ~808nm. The laser beam was then directed into a beta-barium borate crystal, thereby frequency-doubled to ~404 nm to selectively excite the Chl *a* Q_x band. A beam splitter directed a portion of the beam to a sync photodiode (Becker-Hickl, PHD-400) to provide time references to the TCSPC card. The remaining beam, serving as the excitation source, was directed at the adaxial leaf surface at an angle of approximately 70°, carefully avoiding the leaf stem and petioles.

Prior to the measurements, plants were dark-acclimated overnight, and water was added to a custom leaf holder with a water reservoir to maintain leaf hydration throughout the entire measurement. The excitation beam was adjusted to 1.0 mW to saturate the reaction centers. The leaves were treated by one of the three 20-minute actinic light sequences using a Leica KL1500 LCD light source, with high light (HL) set at approximately 1500 μmol m^{-2} s^{-1}. The sequences were designated as following, with the numbers indicating the duration of each high light (HL) or dark (D) period in minutes.

20HL: continuous high light for 20 minutes.

5HL-10D-5HL: 5 minutes of high light, 10 minutes of dark, followed by another 5 minutes of high light.

3HL-1D-1HL-3D-9HL-3D: a more complex sequence combining shorter intervals of high light and dark.

Chl *a* Qy band fluorescence emission was selected at 680 nm by a monochromator (HORIBA Jobin-Yvon; H-20) and detected by a microchannel plate (MCP)-photomultiplier tube (PMT) detector (Hamamatsu R3809U MCP-PMT. The system's instrument response function (IRF) had a full-width half-maximum (FWHM) of ~37 ps, sufficient to resolve sub-nanosecond fluorescence lifetimes. A LabVIEW program was applied to control a series of shutters and coordinate the excitation beam, actinic light, and detector accordingly to the sequences.

Fluorescence decay profiles were recorded over a total integration time of 1 second, from which a 0.2-second timestep with the longest lifetime was selected for analysis to further ensure that the reaction centers were fully saturated[46]. Each fluorescence decay profile was fitted with a bi-exponential decay function and the amplitude-weighted average lifetime was calculated as follows:

$$\tau = \frac{\sum_i A_i \tau_i}{\sum_i A_i} \tag{5}$$

Here, A_i and τ_i denote the amplitudes and fluorescence lifetimes of the i^{th} fitting component, respectively. The lifetime values were directly used in constructing and testing the NPQ model.

Modeling details

NPQ is modeled by a set of differential equations equipped with rate constants, derived from standard rate kinetics on biochemical pathways within the VAZ cycle and a light-dependent quencher activation mechanism.

$$V + P \underset{k_{PV,b}}{\overset{k_{PV,f}}{\rightleftharpoons}} PV \underset{k_{QV,b}}{\overset{k_{QV,f}^{L/D}}{\rightleftharpoons}} QV \tag{6-1}$$

$$A + P \underset{k_{PA,b}}{\overset{k_{PA,f}}{\rightleftharpoons}} PA \underset{k_{QA,b}}{\overset{k_{QA,f}^{L/D}}{\rightleftharpoons}} QA \tag{6-2}$$

$$Z + P \underset{k_{PZ,b}}{\overset{k_{PZ,f}}{\rightleftharpoons}} PZ \underset{k_{QZ,b}}{\overset{k_{QZ,f}}{\rightleftharpoons}} QZ \tag{6-3}$$

$$V + VDE_a \overset{k_{va}}{\rightarrow} A + VDE_a \overset{k_{az}}{\rightarrow} Z + VDE_a \tag{6-4}$$

$$Z \overset{k_{za}}{\rightarrow} A \overset{k_{av}}{\rightarrow} V \tag{6-5}$$

$$PL \underset{k_{QL,b}}{\overset{k_{QL,f}^{\frac{L}{D}}}{\rightleftharpoons}} QL \tag{6-6}$$

$$I \overset{k_{damage}^{L/D}}{\rightarrow} I^* \tag{6-7}$$

We assume Vio, Ant, Zea, and Lut all have some quenching capacity defined by their ability to (1) bind to an antenna complex, forming "PX", (2) activate under light conditions, forming a quencher "QX", and (3) dissipate excitation energy at some rate (κ_{QX}). We assume Lut is always protein-bound. The xanthophyll cycle is mediated by the enzyme VDE, which exists in an active protonated (VDE_a) and de-protonated (VDE_i) state. The model additionally includes the irreversible conversion of functional PSII reaction centers *I* to a damaged state *I**, representing photoinhibition. Explicitly, the kinetic scheme is as follows:

To obtain the model's kinetic differential equation system, each step above is treated as an elementary reaction with rates as given. Details are given in Supplementary Information (Extended methods).

To reduce the number of parameters needed to fit the model, we take VDE concentration to be a ratio $\alpha_{vde_a}(t) = \frac{[VDE_a]}{[VDE_{a,eq}^L]}$ and approximate $k_{va/az}[VDE](t) = k_{va/az,max}^L \cdot \alpha_{vde_a}(t)$. We further model α_{vde} as a dynamic variable with equilibrium $\alpha_{vde,eq}^L = 1$ in light conditions and $\alpha_{vde,eq}^D = \frac{k_{va,max}^D}{k_{va,max}^L}$ in dark conditions:

$$\frac{d\alpha_{vde}}{dt} = k_{VDE}^{L/D}\left(\alpha_{vde,eq}^{L/D} - \alpha_{vde}\right) \tag{7}$$

which simplifies xanthophyll cycle dynamics. Similarly, the rate of damage is modeled as a ratio of damaged cores to the whole pool: $\alpha_{qI}(t) = \frac{I^*}{I+I^*}$. Photoinhibition is thus modeled as the irreversible accumulation of α_{qI}, whose rate is proportional to τ_F:

$$\frac{d\alpha_{qI}}{dt} = k_{damage}^{L/D} * \left(1 - \alpha_{qI}\right) * \tau_F \quad (8)$$

Hence a decrease in lifetime (as defined in Results) decreases the rate of photoinhibition. The complete model is able to predict dynamic concentrations of the various carotenoid quenchers, enzyme activation kinetics, and the rate and extent of damage from photoinhibition.

Rate constants and initial concentrations (mmol/mol Chl *a*) of violaxanthin and membrane protein binding sites are additional parameters fit to data. The fit quality of a parameter set, $\delta^2(\theta)$, is quantified by performing a least-squares residual fit to experimental lifetime data for a given D-L sequence S:

$$\delta^2(\theta) = \sum_{i=1}^{N_{snaps}} \left(\tau_{exp}\left(t_i, S_i\right) - \tau_{model}\left(t_i, S_i, \theta\right)\right)^2 \quad (9)$$

The differential equation set is solved with MATLAB ode23t. *particleswarm* from the MATLAB Global Optimization Toolbox is used to perform particle swarm optimization searching parameter space for fit quality minima. The output Θ is refined using *patternsearch* and *fminsearch*.

DATA AVAILABILITY

The datasets generated and/or analyzed during the current study are available from the corresponding author upon reasonable request and will be provided upon final submission.

CODE AVAILABILITY

The codes used in this study are available from the corresponding author upon reasonable request and will be provided upon final submission.

COMPETING INTERESTS

The authors declare no competing interests.

ACKNOWLEDGMENTS

We thank Dr. Thomas P. Fay for kindly providing codes from the previous studies and insight on modeling based on the xanthophyll cycle. We thank Dr. Masakazu Iwai for his insights on HPLC measurements. This work was supported by the U.S. Department of Energy, Office of Science, through the Photosynthetic Systems program in the Office of Basic Energy Sciences. R.L. was supported in part by the U.S. Department of Energy, Office of Science, Office of Workforce Development for Teachers and Scientists (WDTS) under the Science Undergraduate Laboratory Internships (SULI) program. D.P.T. was supported by the Berkeley Fellowship and the NSF Graduate Research Fellowship Program (Grant DGE 1752814). K.K.N. is an investigator of the Howard Hughes Medical Institute.

AUTHOR CONTRIBUTIONS

L.L. and R.L. contributed equally. G.R.F. and L.L. conceived the research. D.P.-T. and S.A.M. generated and screened for *N. benthamiana* NPQ mutants. L.L. conducted the TCSPC experiments and initial data analysis, with technical assistance from H.E.L., A.M., and R.L. L.L. performed HPLC experiments and analysis with input from D.P.-T. and H.H. R.L. and T.-Y.L. developed the model, with R.L. implementing it and performing the final data analysis. L.L., R.L., and G.R.F. drafted the manuscript with input from D. P.-T., K.K.N. and T.-Y.L.

REFERENCES

1. Dekker, J. P. & Van Grondelle, R. Primary charge separation in Photosystem II. *Photosynth Res* **63**, 195–208 (2000).

2. Peterman, E. J., Dukker, F. M., van Grondelle, R. & van Amerongen, H. Chlorophyll a and carotenoid triplet states in light-harvesting complex II of higher plants. *Biophys J* **69**, 2670–2678 (1995).
3. Ledford, H. K. & Niyogi, K. K. Singlet oxygen and photo-oxidative stress management in plants and algae. *Plant, Cell & Environment* **28**, 1037–1045 (2005).
4. Mansoor, S. *et al.* Reactive Oxygen Species in Plants: From Source to Sink. *Antioxidants (Basel)* **11**, 225 (2022).
5. Demmig-Adams, B. & Adams III, W. W. Photoprotection in an ecological context: the remarkable complexity of thermal energy dissipation. *New Phytologist* **172**, 11–21 (2006).
6. Bassi, R. & Dall'Osto, L. Dissipation of Light Energy Absorbed in Excess: The Molecular Mechanisms. *Annu. Rev. Plant Biol.* **72**, 47–76 (2021).
7. Müller, P., Li, X.-P. & Niyogi, K. K. Non-Photochemical Quenching. A Response to Excess Light Energy. *Plant Physiology* **125**, 1558–1566 (2001).
8. Li, X.-P. *et al.* Regulation of Photosynthetic Light Harvesting Involves Intrathylakoid Lumen pH Sensing by the PsbS Protein. *Journal of Biological Chemistry* **279**, 22866–22874 (2004).
9. Demmig-Adams, B. *et al.* Modulation of PsbS and flexible vs sustained energy dissipation by light environment in different species. *Physiologia Plantarum* **127**, 670–680 (2006).
10. Niyogi, K. K., Grossman, A. R. & Björkman, O. Arabidopsis mutants define a central role for the xanthophyll cycle in the regulation of photosynthetic energy conversion. *Plant Cell* **10**, 1121–1134 (1998).
11. Demmig-Adams, B., Stewart, J. J., López-Pozo, M., Polutchko, S. K. & Adams, W. W. Zeaxanthin, a Molecule for Photoprotection in Many Different Environments. *Molecules* **25**, 5825 (2020).
12. Pogson, B., McDonald, K. A., Truong, M., Britton, G. & DellaPenna, D. Arabidopsis carotenoid mutants demonstrate that lutein is not essential for photosynthesis in higher plants. *Plant Cell* **8**, 1627–1639 (1996).

13. Pogson, B. J., Niyogi, K. K., Björkman, O. & DellaPenna, D. Altered xanthophyll compositions adversely affect chlorophyll accumulation and nonphotochemical quenching in *Arabidopsis* mutants. *Proc. Natl. Acad. Sci. U.S.A.* **95**, 13324–13329 (1998).
14. Jahns, P. & Holzwarth, A. R. The role of the xanthophyll cycle and of lutein in photoprotection of photosystem II. *Biochimica et Biophysica Acta (BBA) - Bioenergetics* **1817**, 182–193 (2012).
15. Xu, P., Tian, L., Kloz, M. & Croce, R. Molecular insights into Zeaxanthin-dependent quenching in higher plants. *Sci Rep* **5**, 13679 (2015).
16. Nilkens, M. *et al.* Identification of a slowly inducible zeaxanthin-dependent component of non-photochemical quenching of chlorophyll fluorescence generated under steady-state conditions in Arabidopsis. *Biochimica et Biophysica Acta (BBA) - Bioenergetics* **1797**, 466–475 (2010).
17. Bellafiore, S., Barneche, F., Peltier, G. & Rochaix, J.-D. State transitions and light adaptation require chloroplast thylakoid protein kinase STN7. *Nature* **433**, 892–895 (2005).
18. Long, S. P., Humphries, S. & Falkowski, P. G. Photoinhibition of Photosynthesis in Nature. *Annual Review of Plant Biology* **45**, 633–662 (1994).
19. Steen, C. J., Morris, J. M., Short, A. H., Niyogi, K. K. & Fleming, G. R. Complex Roles of PsbS and Xanthophylls in the Regulation of Nonphotochemical Quenching in *Arabidopsis thaliana* under Fluctuating Light. *J. Phys. Chem. B* **124**, 10311–10325 (2020).
20. Short, A. H. *et al.* Xanthophyll-cycle based model of the rapid photoprotection of *Nannochloropsis* in response to regular and irregular light/dark sequences. *The Journal of Chemical Physics* **156**, 205102 (2022).
21. Short, A. *et al.* Kinetics of the xanthophyll cycle and its role in photoprotective memory and response. *Nat Commun* **14**, 6621 (2023).
22. Litvín, R., Bína, D., Herbstová, M. & Gardian, Z. Architecture of the light-harvesting apparatus of the eustigmatophyte alga Nannochloropsis oceanica. *Photosynth Res* **130**, 137–150 (2016).

23. Vieler, A. *et al.* Genome, Functional Gene Annotation, and Nuclear Transformation of the Heterokont Oleaginous Alga Nannochloropsis oceanica CCMP1779. *PLoS Genet* **8**, e1003064 (2012).
24. Buck, J. M. *et al.* Lhcx proteins provide photoprotection via thermal dissipation of absorbed light in the diatom Phaeodactylum tricornutum. *Nat Commun* **10**, 4167 (2019).
25. Lee, T.-Y. *et al.* Chlorophyll to zeaxanthin energy transfer in nonphotochemical quenching: An exciton annihilation-free transient absorption study. *Proceedings of the National Academy of Sciences* **121**, e2411620121 (2024).
26. Tian, Y., Sacharz, J., Ware, M. A., Zhang, H. & Ruban, A. V. Effects of periodic photoinhibitory light exposure on physiology and productivity of Arabidopsis plants grown under low light. *J Exp Bot* **68**, 4249–4262 (2017).
27. Long, S. P. *et al.* Into the Shadows and Back into Sunlight: Photosynthesis in Fluctuating Light. *Annu. Rev. Plant Biol.* **73**, 617–648 (2022).
28. Zhu, X., Ort, D. R., Whitmarsh, J. & Long, S. P. The slow reversibility of photosystem II thermal energy dissipation on transfer from high to low light may cause large losses in carbon gain by crop canopies: a theoretical analysis. *Journal of Experimental Botany* **55**, 1167–1175 (2004).
29. Li, Z. *et al.* Lutein Accumulation in the Absence of Zeaxanthin Restores Nonphotochemical Quenching in the Arabidopsis thaliana npq1 Mutant. *Plant Cell* **21**, 1798–1812 (2009).
30. Niyogi, K. K. *et al.* Photoprotection in a zeaxanthin- and lutein-deficient double mutant of Arabidopsis. *Photosynthesis Research* **67**, 139–145 (2001).
31. Carbonera, D., Agostini, A., Bortolus, M., Dall'Osto, L. & Bassi, R. Violaxanthin and Zeaxanthin May Replace Lutein at the L1 Site of LHCII, Conserving the Interactions with Surrounding Chlorophylls and the Capability of Triplet–Triplet Energy Transfer. *International Journal of Molecular Sciences* **23**, 4812 (2022).

32. Pogson, B., McDonald, K. A., Truong, M., Britton, G. & DellaPenna, D. Arabidopsis carotenoid mutants demonstrate that lutein is not essential for photosynthesis in higher plants. *Plant Cell* **8**, 1627–1639 (1996).

33. Nicol, L., Nawrocki, W. J. & Croce, R. Disentangling the sites of non-photochemical quenching in vascular plants. *Nat. Plants* **5**, 1177–1183 (2019).

34. Leuenberger, M. *et al.* Dissecting and modeling zeaxanthin- and lutein-dependent nonphotochemical quenching in *Arabidopsis thaliana*. *Proc. Natl. Acad. Sci. U.S.A.* **114**, (2017).

35. Kromdijk, J. *et al.* Improving photosynthesis and crop productivity by accelerating recovery from photoprotection. *Science* **354**, 857–861 (2016).

36. De Souza, A. P. *et al.* Soybean photosynthesis and crop yield are improved by accelerating recovery from photoprotection. *Science* **377**, 851–854 (2022).

37. Garcia-Molina, A. & Leister, D. Accelerated relaxation of photoprotection impairs biomass accumulation in Arabidopsis. *Nat Plants* **6**, 9–12 (2020).

38. Lehretz, G. G., Schneider, A., Leister, D. & Sonnewald, U. High non-photochemical quenching of VPZ transgenic potato plants limits CO_2 assimilation under high light conditions and reduces tuber yield under fluctuating light. *JIPB* **64**, 1821–1832 (2022).

39. Croce, R. *et al.* Perspectives on improving photosynthesis to increase crop yield. *The Plant Cell* **36**, 3944–3973 (2024).

40. Zaks, J., Amarnath, K., Kramer, D. M., Niyogi, K. K. & Fleming, G. R. A kinetic model of rapidly reversible nonphotochemical quenching. *Proceedings of the National Academy of Sciences* **109**, 15757–15762 (2012).

41. Ruban, A. V. Crops on the fast track for light. *Nature* **541**, 36–37 (2017).

42. Shuang, S.-P. *et al.* A Comparison of Photoprotective Mechanism in Different Light-Demanding Plants Under Dynamic Light Conditions. *Front. Plant Sci.* **13**, 819843 (2022).

43. Patel-Tupper, D. *et al.* Multiplexed CRISPR/Cas9 mutagenesis of rice PSBS1 non-coding sequences for transgene-free overexpression. 2023.10.20.563333 Preprint at https://doi.org/10.1101/2023.10.20.563333 (2023).
44. Fraser, P. D. *et al.* Manipulation of Phytoene Levels in Tomato Fruit: Effects on Isoprenoids, Plastids, and Intermediary Metabolism. *The Plant Cell* **19**, 3194–3211 (2007).
45. Gupta, P., Sreelakshmi, Y. & Sharma, R. A rapid and sensitive method for determination of carotenoids in plant tissues by high performance liquid chromatography. *Plant Methods* **11**, 5 (2015).
46. Sylak-Glassman, E. J., Zaks, J., Amarnath, K., Leuenberger, M. & Fleming, G. R. Characterizing non-photochemical quenching in leaves through fluorescence lifetime snapshots. *Photosynth Res* **127**, 69–76 (2016).

Tables

Table 1 Summary of *N. benthamiana* mutants used in this study.

Genotype	***NPQ Phenotype***		**References**
WT	Wild type		
npq4	Lacks PsbS	No qE	(Lee et al., 2024)
npq1	Lacks VDE	No Ant or Zea	(Lee et al., 2024)
lut2	Lacks Lut	No qE from Lut	(Lee et al., 2024)
zep2	Reduced ZEP	Accumulates Zea	Generated in this study
npq4 npq1	Lacks VDE and PsbS	No qE or qZ	Generated in this study
npq1 lut2	Lacks VDE and Lut	No qZ, has qE only from Vio	Generated in this study
npq4 lut2	Lacks PsbS and lutein	No qE	Generated in this study
npq4 zep2	Lacks PsbS and reduced ZEP	No qE and accumulates Zea	Generated in this study
zep2 lut2	Reduced ZEP and lacks Lut	No qE from Lut and accumulates Zea	Generated in this study

Table 2 Quenching efficiencies of Lut (QL), Vio (QV), Ant (QA), and Zea via qE (QZ) and Zea via qZ (qZ).

Species	Q_{eff}
QV	0.0009
QA	0.0029
QZ	0.0328
QL	0.0033
qZ	0.0330

Quenching efficiencies were calculated by $Q_{eff} = \frac{k_{pxf}}{k_{pxf}+k_{pxb}} \cdot \frac{k_{qxf}}{k_{qxf}+k_{qxb}} \cdot \kappa_{QX}$, where $\frac{k_{pxf}}{k_{pxf}+k_{pxb}} \cdot \frac{k_{qxf}}{k_{qxf}+k_{qxb}}$ represents the effective maximum fraction of molecules of xanthophyll in a given pool contributing to quenching.

Figures

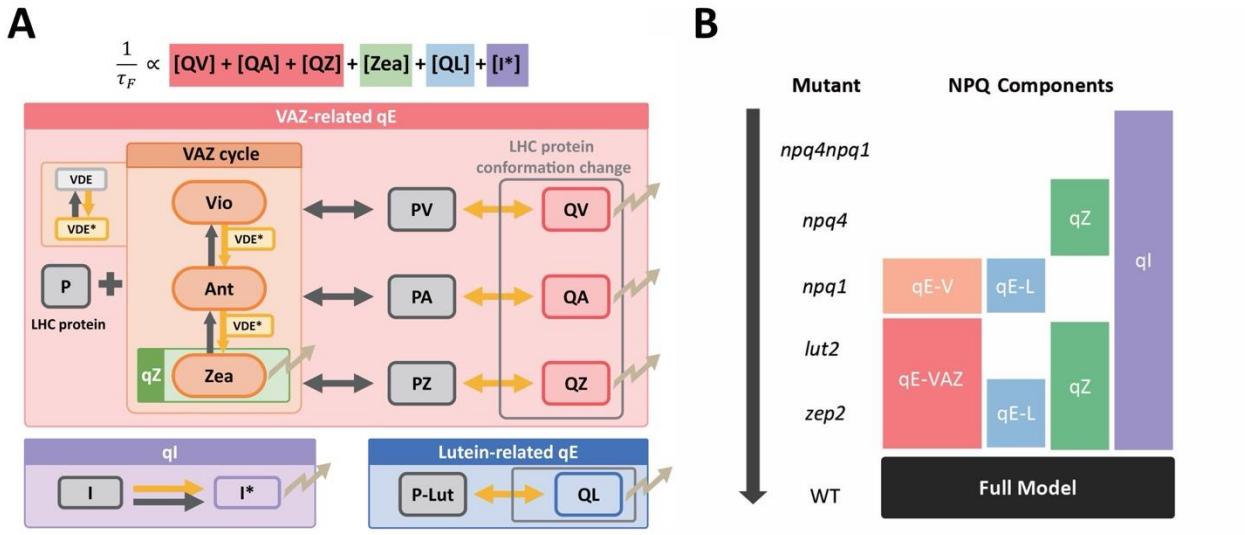

Fig. 1 Schematic of the stepwise parameterization of the NPQ model.

A Schematic of the NPQ Model constructed from qE, qZ, and qI components, including the VAZ cycle and lutein activation. The model captures interconversion of Vio, Ant, and Zea and its binding to an LHC protein P (Lut is assumed to be always bound) as indicated by the protein-bound PX state and high light dependent activation to its respective quenching QX state. Here, X is an interchangeable xanthophyll, and the activation of PX to QX is depicted. Arrows represent rate-dependent processes modeled using differential rate law kinetics. Light-independent and light-dependent processes are indicated by black and yellow arrows, respectively. Quenching processes (↯) are modeled using an inverse relation between chlorophyll fluorescence lifetime τ_F and the amount of each quenching species.

B Schematic of stepwise training of the NPQ model by decomposition into components using NPQ mutants. The black arrow indicates the sequential fitting of model rate parameters, starting with the simplest mutant (*npq4npq1*) and progressively incorporating additional NPQ components to parameterize the full wild-type (WT) model.

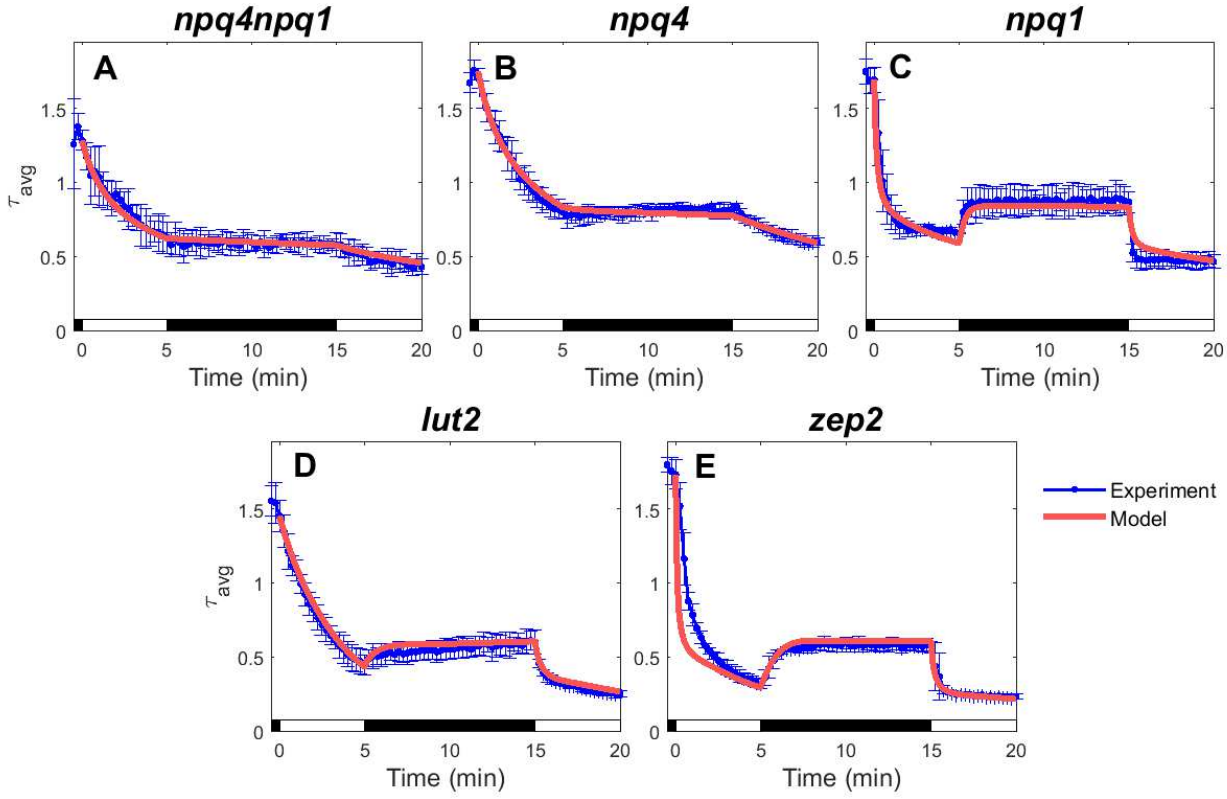

Fig. 2 Whole leaf chlorophyll fluorescence lifetime data (blue) and model fitting (red) under the 5HL-10D-5HL sequence for mutants used to train model parameters. The model was fitted using fluorescence lifetime data of **A** *npq4npq1* (*n*=3), **B** *npq4* (*n*=3), **C** *npq1* (*n*=3), **D** *lut2* (*n*=3), and **E** *zep2* (*n*=4) leaves. Model fitting was performed with lifetime data under this sequence together with the 3HL-1D-1HL-3HL-9D-3HL sequence (Figure S4). RMSD of fittings are (s^{-1}): **A** 0.027, **B** 0.043, **C** 0.125, **D** 0.142, **E** 0.239. White and black bars indicate high light (HL) and dark (D) phases of the actinic light sequence. Error bars represent ± 2 SE from *n* biological replicates.

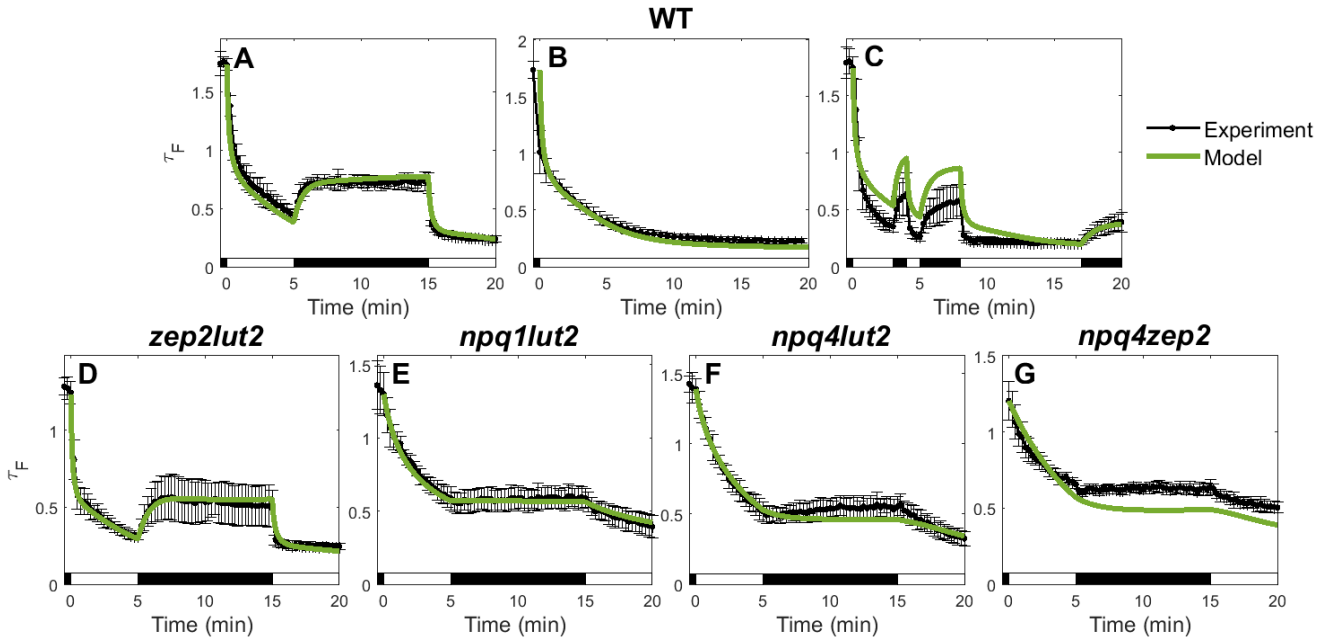

Fig. 3 Whole leaf chlorophyll fluorescence lifetime data (black) and model (green) predictions. Model predicted τ_F behaviors were generated for WT under three light sequences: **A** 5HL-10D-5HL (*n*=3), **B** 20HL (*n*=6), **C** 3HL-1D-1HL-3D-9HL-3D (*n*=3), and for double mutants under the 5HL-10D-5HL sequence: **D** *zep2lut2* (*n*=5), **E** *npq1lut2* (*n*=4), **F** *npq4lut2* (*n*=3), **G** *npq4zep2* (*n*=5). Model predictions were calculated from parameters fitted in Figure 2 and Figure S4, with $[V]_{0,WT}$ fit separately to account for differences in $[V]_0$ observed in HPLC measurements. For double mutants (**D-G**), mutant-specific parameters are combined to produce the modeled result. Error bars represent ± 2 SE from *n* biological replicates. RMSD (s^{-1}) = **A** 0.182, **B** 0.935, **C** 0.811, **D** 0.269, **E** 0.023, **F** 0.214, **G** 0.377. White and black bars indicate high light (HL) and dark (D) phases of the actinic light sequence. Error bars represent ± 2 SE from *n* biological replicates.

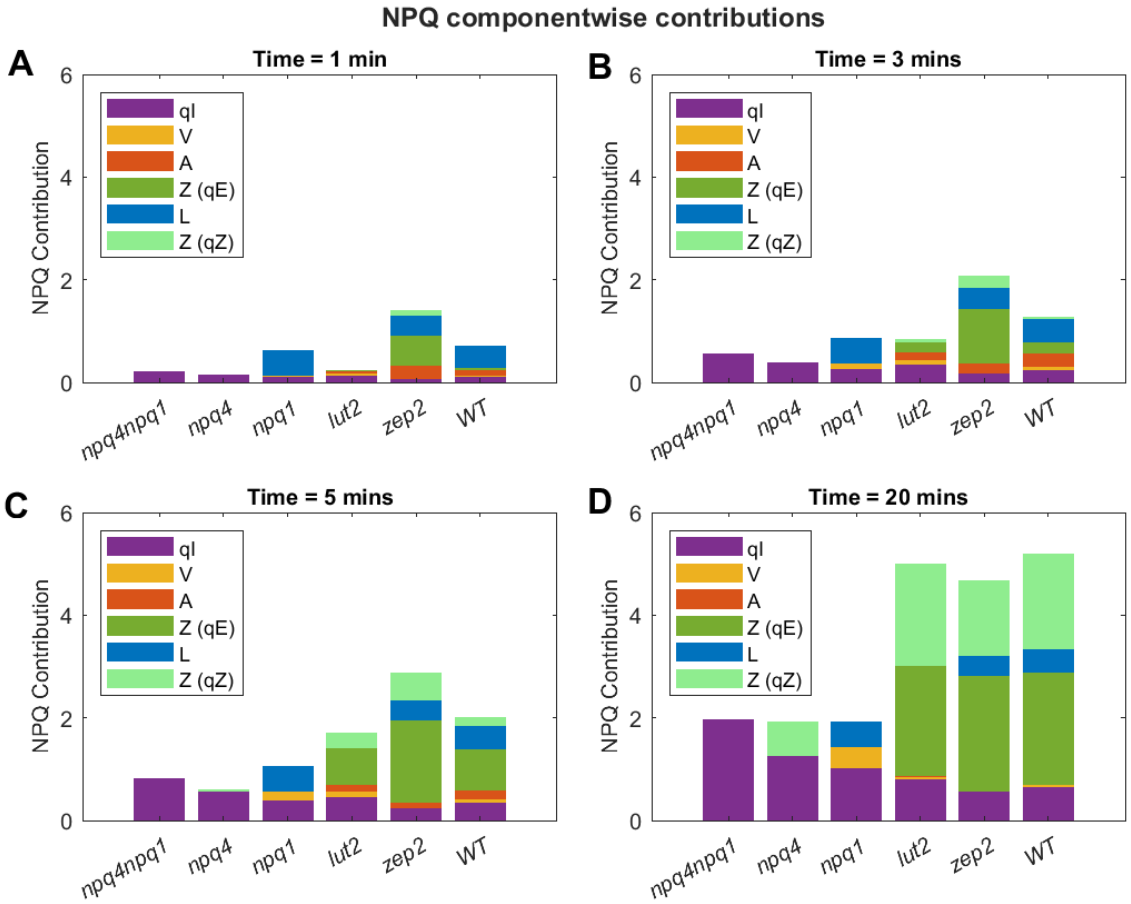

Fig. 4 The NPQ contributions of qI, qE (V/A/Z/L), and qZ quenching components in *npq4npq1/npq4/npq1/lut2/zep2*/WT under continuous high light at A t=1 min, **B** t=3 mins, **C** t=5 mins, **D** t=20 mins. The NPQ contribution for each component was quantified by the linear relation $\kappa_{qX} \cdot [QX](t)$ for each quenching xanthophyll QX, $\kappa_{qZ} \cdot [Z](t)$ for qZ, and $\kappa_{qI} \cdot \alpha_{qI}(t)$ for qI.

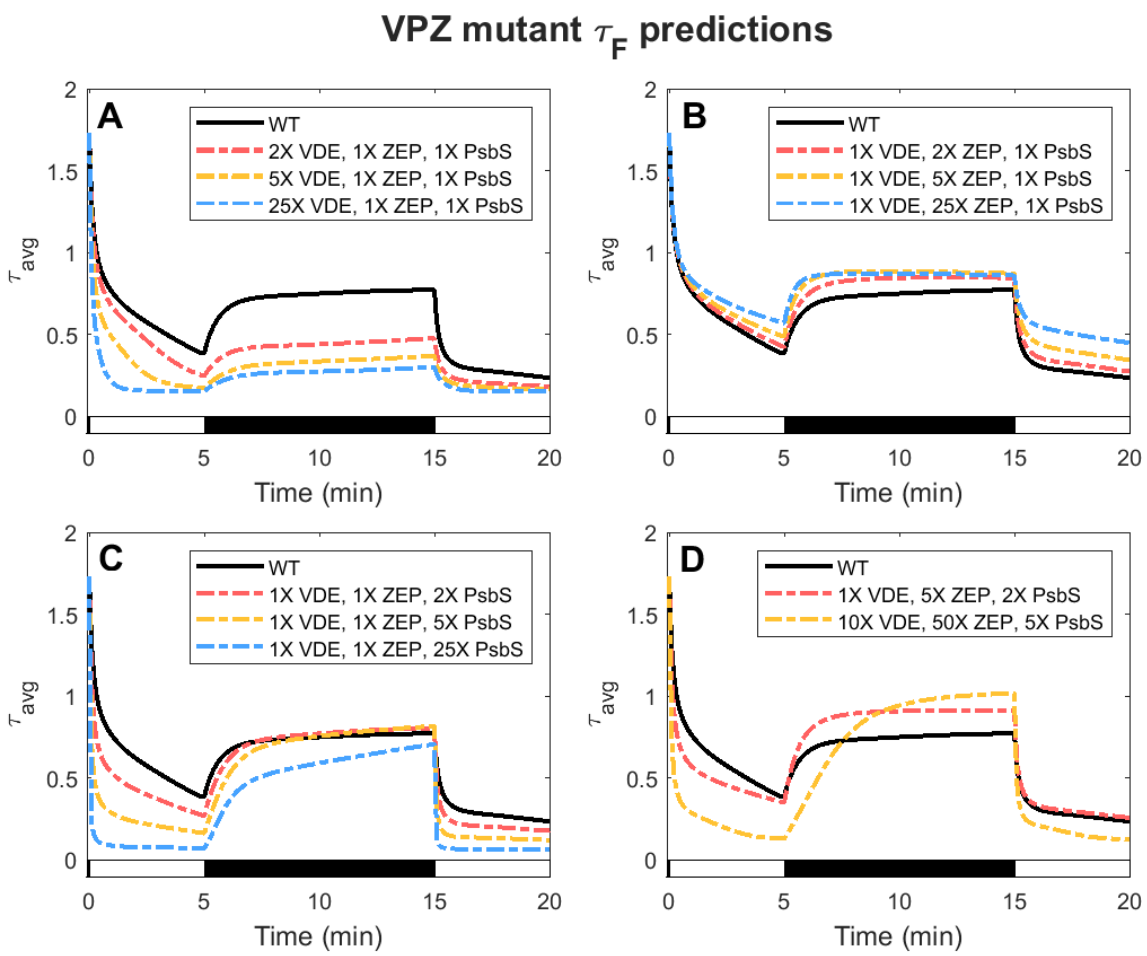

Fig. 5 Model predictions for τ_F dynamics in logically constructed overexpression mutants under the 5HL-10D-5HL light sequence. A VDE activity upregulated by 2X, 5X, and 25X from WT. **B** ZEP activity upregulated by 2X, 5X, and 25X from WT. **C** PsbS activity upregulated by 2X, 5X, and 25X from WT. **D** Combined modeled upregulation of VDE, ZEP, and PsbS: VDE activity upregulated by 1X and 10X, ZEP activity upregulated by 5X and 50X, and PsbS activity upregulated by 2X and 5X. White and black bars indicate high-light (HL) and dark (D) phases of the actinic light sequence.

Supplementary Files

This is a list of supplementary files associated with this preprint. Click to download.

- Finalv8SItobaccomodeling.pdf
- MovieS1.gif